Maritime surveillance radar
Part 1: Radar scattering from the ocean surface

K.D. Ward, MA, PhD, CEng, MIEE
C.J. Baker, BSc, PhD, DipAppPhys
S. Watts, MA, MSc, PhD, CEng, MIEE

Indexing terms: Radar, Maritime surveillance, Clutter, Modelling

Abstract: The successful optimisation of the detection performance of maritime surveillance radars requires a detailed knowledge and understanding of both forward- and backscattering from the ocean surface. Such an understanding enables the development of suitable signal-processing techniques. The paper is therefore divided into two parts, the first being concerned with radar scattering from an ocean environment and the second with target detection. In the first part it is shown, through the analysis of full-scale measurements, how the amplitude and correlation properties of high-resolution radar backscatter (sea clutter) can be accurately represented by the compound K-distribution model which has the unique characteristic of providing realistic performance predictions for a wide range of signal-processing techniques. Although the model has been presented before, the paper gives the first detailed account of the evidence and statistical analysis which have led to the model. In addition to modelling noncoherent clutter it is shown how the spectral and polarisation characteristics of coherently detected sea clutter relate to those observed in the noncoherent case. Results are also presented of forward-scattering and multipath propagation. This includes a consideration of the importance of the spatial and temporal coherence of the forward-scattered wavefront.

1 Introduction

In this paper the statistics of radar scattering from the sea surface are considered in terms of their relevance to the operation of maritime surveillance radar. The descriptions are based upon experimental observations, and the statistical models that are developed are aimed at encapsulating all the information necessary to successfully predict radar performance. For the most part the compound K-distribution is used. This model has been presented and applied in previous publications [e.g. 1, 2]. The purpose of this paper is to summarise all the results obtained to date, to present a more complete set of evidence supporting the validity of the model than has previously been possible, and to extend the work to coherent clutter and multipath propagation. Part 2 of the paper covers application to the assessment of radar performance and the derivation of processing techniques [3]. It is in Part 2 that the full significance of such aspects as correlation become evident, thus demonstrating the value of this type of model over existing amplitude distribution descriptions.

When a radar has a spatial resolution high enough to resolve structure on the sea surface, the sea clutter received by the system is not well modelled by a Gaussian process. Previous work on understanding the non-Gaussian nature of sea clutter has concentrated on the amplitude distribution and on the shape of the average power spectrum. These two properties are sufficient to describe a Gaussian process, because of the factorisation of the higher order statistics. In general, however, they provide an incomplete description of non-Gaussian processes, and may result in modelling that omits features of importance concerning the effects of the non-Gaussian nature. This is the case for sea clutter, where correlation properties not evident in the average power spectrum (nor in the complex autocorrelation function, which is equivalent) severely affect radar performance and signal processing optimisation. To overcome this problem, a programme of work looking at the non-Gaussian nature of high resolution sea clutter has resulted in a model known as the compound K-distribution. This model is most directly applicable to real-beam radar noncoherent clutter, but is being extended to apply to coherent clutter. Extension to synthetic aperture radar (SAR) is foreseen in the future.

Forward scattering from the sea surface is also important to the understanding of surveillance radar performance [4]. The principal effect is the interference between the direct and indirect illumination of targets which causes fluctuations in target echoing areas and high resolution signatures. To describe these effects, work has been undertaken to characterise the spatial and temporal properties of the forward-scattered wavefront from the sea surface. The results can be applied to radar target modelling and radar performance assessment [5].

As indicated in the opening sentence of this paper, we are concentrating on the statistics of observed radar scattering effects. In that sense our descriptions are phenomenological rather than based upon the mechanisms of the electromagnetic rough-surface interactions. The reasons for this are twofold. First, we wish to solve the problem of improving maritime surveillance radars in the most

Paper 7150F (E15), first received 5th July 1989 and in revised form 2nd January 1990

Dr. Ward and Dr. Baker are with the Procurement Executive, Ministry of Defence, Royal Signals & Radar Establishment, St. Andrews Road, Great Malvern, Worcs. WR14 3PS, United Kingdom
Dr. Watts is with THORN EMI Electronics Ltd., 248 Blyth Road, Hayes, Middlesex UB3 1HR, United Kingdom

efficient manner. Secondly, there is a wide body of evidence that a very broad range of problems can be solved purely by observing statistics. This is most well known for cases where the central limit theorem applies, but in recent years it has been found that considerable progress can be made in non-Gaussian problems without resorting to exact application-specific solutions [6]. A problem with this approach is that it does not lend itself to remote sensing, where one is aiming to deduce characteristics of the scattering surface from the scattered radiation. Because of this we are trying to extend our phenomenological models towards a more mechanistic description, but this area is only mentioned briefly in this paper.

Most of the results presented in the paper relate to measurements made by radars operating at X-band (9.5–10 GHz). The systems use a pulsed waveform with a 50 MHz FM modulation within the pulse, which gives a range resolution of approximately 4 m. Pulse-to-pulse frequency agility is often used, where the transmitted frequency is stepped by the pulse bandwidth from pulse to pulse over a 500 MHz radar bandwidth. The systems use antennas giving 1.2° beamwidth, which means that the across range resolution is dependent upon range. Generally speaking measurements are usually made 'search-lighting' an area of sea. Range profiles are recorded, thereby allowing both the temporal and spatial correlation properties of the backscatter to be determined simultaneously. Recordings are possible of coherent and polarimetric properties. For the former the radar is phase coherent from pulse to pulse and records in-phase and quadrature detected signals. For the latter there is pulse-to-pulse switching between orthogonal polarisation on the transmitter, and a two-channel receiver to enable the recording of the full coherent polarisation scattering matrix.

2 Noncoherent high-resolution sea clutter

A large proportion of radars use only the envelope of the received signal in their processing. Since they do not use the signal phase, these systems can be noncoherent from pulse to pulse, and in consequence can use simple transmitters such as pulsed magnetrons. These radars, particularly if they are high resolution, often suffer from 'spiky' sea clutter. This is a term applied to non-Rayleigh clutter when the probability of the signal crossing a threshold is much higher than would be expected from a Rayleigh distribution given the clutter power. The clutter has the property that threshold crossings tend to occur in the same place on the radar display, thus indicating important long term correlation properties.

2.1 The compound K-distribution

Fig. 1 shows the time history, of an individual range cell, of the envelope demodulated signal from a radar looking at the sea at a grazing angle of approximately one degree, with vertical polarisation. The plot shows the principal features of high-resolution radar sea clutter. There is a fast fluctuation from pulse to pulse which is apparently modulated by an underlying structure. Comparison of fixed frequency and frequency agility records show that the fast fluctuation decorrelates from pulse to pulse with frequency agility and is correlated for between 5 and 10 ms on a fixed frequency. The underlying structure is unaffected by frequency agility and generally fluctuates on a timescale of the order of seconds. The temporal and spatial correlation of the modulation is very dependent on the radar parameters, the viewing angles and the environmental conditions.

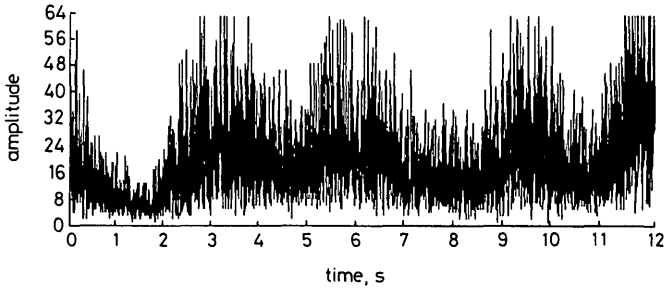

Fig. 1 *Time history of vertically polarised sea clutter, showing the two fluctuation components*

The presence of the fast fluctuation, and its decorrelation with change in frequency, implies that many scatterers contribute within each illuminated patch. This is confirmed when it is found that the clutter amplitude is locally Rayleigh distributed, which results from the central limit applying within the patch. It suggests that the non-Rayleigh nature of the overall clutter amplitude distribution is due to bunching of scatterers by the sea wave structure, rather than being due to a small number of effective scatterers. The Rayleigh distribution for the speckle is illustrated in Fig. 2 where the cumulative dis-

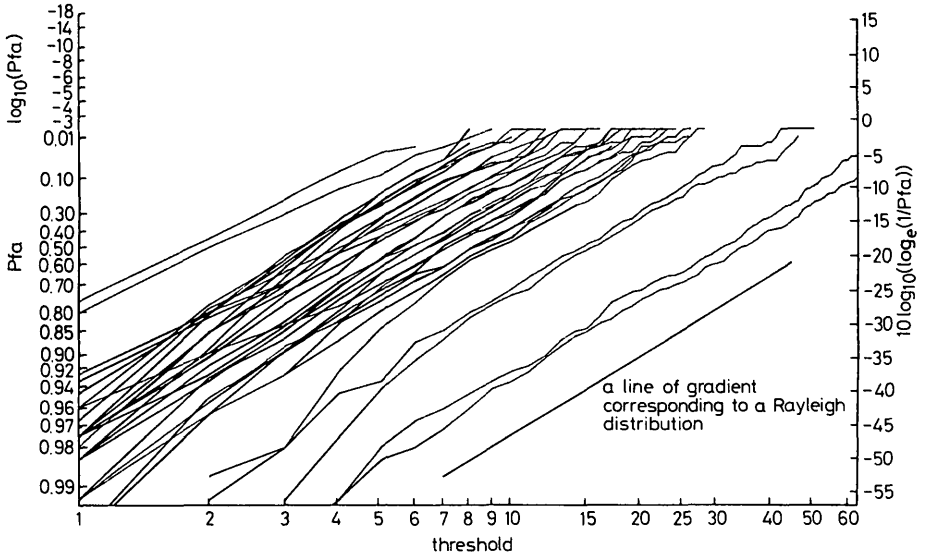

Fig. 2 *Pulse to pulse distributions of individual range cells taken over 240 ms*
Vertical polarisation; frequency agility; Weibull paper

tributions of 250 ms time sequences are plotted on 'Weibull' paper. Here a Rayleigh distribution corresponds to a line of gradient 2, and the intercept is indicative of the sample mean. Fig. 2 shows that the time sequences each have Rayleigh distributed amplitudes; the horizontal displacements of the plots are due to the modulation changing between sequences. The plots to the right of the figure correspond to high local means, which are often referred to as sea spikes.

It is thus demonstrated that the clutter may be described by a modulated Gaussian process. Values of the modulation are obtained from the data by averaging over 250 ms to remove speckle fluctuations. The distribution of the second component may then be obtained. From analysis it is found that the intensity of the modulations is gamma distributed, with the shape parameter dependent on the radar and environmental parameters. This is demonstrated in Figs. 3*a* and *b* where the normalised intensity moments of the modulation of many records of vertically and horizontally polarised clutter are compared to those of a gamma distribution.

Combining the modulation and speckle terms results in the K-distribution for overall clutter amplitude given by

$$p(a) = \frac{2b}{\Gamma(v)}\left(\frac{ba}{2}\right)^{v} K_{v-1}(ba) \tag{1}$$

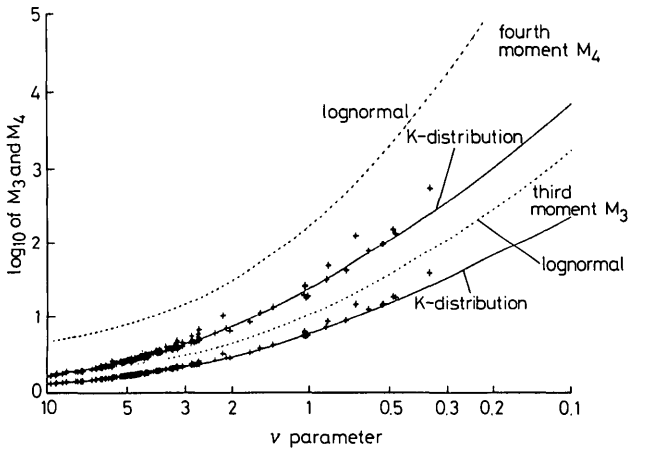

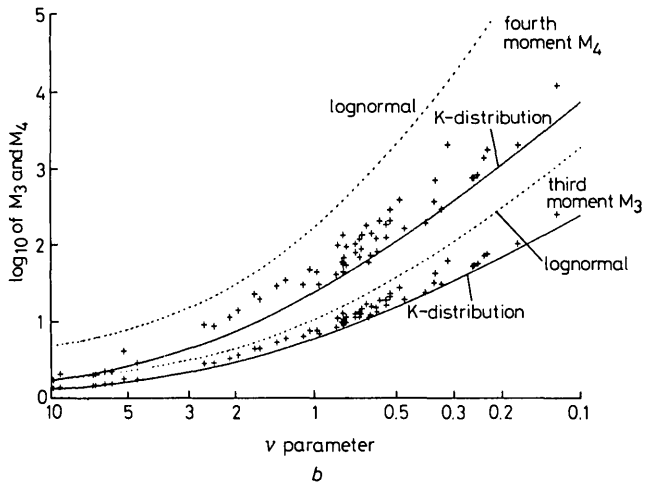

Fig. 3 *Moments of the underlying modulation of many airborne sea clutter measurements*

The plotted curves show moments of modulation corresponding to the overall pulse-to-pulse distributions as labelled, i.e. moments corresponding to the gamma distribution of modulation are labelled as the K-distribution. Experimental results are shown as +. $M_2 = 1 + 1/v$

a Vertical polarisation

b Horizontal polarisation

where a is the clutter amplitude, b is a scale parameter and v is a shape parameter.

The significance of this model is that the non-Rayleigh amplitude distribution may be separated into the two components which, because of their spatial and temporal correlation properties, need to be introduced at different stages in the evaluation of signal-processing performance. The improvement in accuracy of this method over the Gaussian method, when applied to non-Gaussian statistics as discussed earlier, is considerable [1].

2.2 Gamma distribution for the underlying modulation

Whilst the origin of the Rayleigh distribution for the speckle component is clear (the central limit theorem), the reason for the gamma distribution providing a good model for the underlying modulation is less obvious. Arguments based on the detailed characteristics of the sea surface and the interaction of the electromagnetic waves with this type of surface become less attractive when it is found that the compound K-distribution is also a good model for texture in SAR images of land [7]. In addition, the K-distribution describes the amplitude scintillations caused by the atmosphere on starlight, and the scattering of laser light by dynamic liquid crystals and thermal plumes of air [6]. In the light of this evidence, theoretical work has resulted in a number of models for the origin of the K-distribution: the bunching of scatterers caused by a birth-death-migration process [9] and the gamma distribution as the first term in a Laguerre series expansion of the modulation PDF [8].

A more general approach is developed in the following few paragraphs. This shows that the gamma distribution is an approximation, in fact slightly underestimating the moments, to a bunching of scatters which is insensitive of the type of correlation present. Consider a surface which has a PDF of local reflectivity y, for an integrated area a, given by $p_a(y)$. If there is no spatial correlation, the PDF for an integrated area $2a$ is given by the convolution of $p_a(y)$ with itself. Thus

$$p_{2a}(y) = p_a(y) \otimes p_a(y) \tag{2}$$

This may be evaluated using the Fourier transform of the PDF, which is known as the characteristic function $Q(s)$. Thus

$$Q_{2a}(s) = Q_a^2(s) \tag{3}$$

This can usefully be expressed in terms of the cumulants K_i where

$$K_i = \frac{\partial^i}{\partial s^i} \log_e Q(s)\bigg|_{s=0} \tag{4}$$

i.e. K_i are the coefficients of $s^i/i!$ in the expansion of $\ln Q(s)$. When two variates are added, as in the change of area from a to $2a$, the cumulants of the new PDF are the sum of the respective cumulants of the variates' PDFs:

$$K_{i(2a)} = 2K_{i(a)} \tag{5}$$

The cumulants scale in the same way as the moments and can therefore be normalised:

$$K_{i(norm)} = \frac{K_i}{(K_1)^i} \tag{6}$$

Consider a distribution family that is characterised by a function with two free parameters: a scale parameter that defines the mean, and a shape parameter that defines the

normalised variance. K_1 and K_2 are then defined by the scale and shape parameters, and the remaining cumulants are fixed functions of these.

When n variates are added together the resulting PDF remains in the same distribution family if, and only if, the cumulants (for $i \geqslant 3$) of the family can be expressed in a form that is independent of n, which implies that

$$K_{i(norm)} = F_i K_{2(norm)}^{i-1} \quad \text{for } i \geqslant 3 \tag{7}$$

where the F_i are constant within the family.

This is a definition of an infinitely divisible family. The gamma distribution obeys this criterion because

$$K_i = (i-1)!\nu \tag{8}$$

and therefore

$$F_i = (i-1)! \tag{9}$$

Thus, if the surface reflectivity has a gamma distribution at very high resolution, and if it is spatially uncorrelated, it will remain gamma distributed for all resolutions. At low resolution the distribution tends to a delta function. This is due to $K_{i(norm)}$ decreasing as $(\text{area})^{-i}$ until only K_1 remains. If the normalisation is performed relative to K_2, (the variance), the reduction in the higher cumulants results in a distribution where all K_i, for i greater than 2, are zero. This is a Gaussian distribution, the above being a simple illustration of the central limit theorem. We normalise to K_1 (the mean) because the reflectivity is always positive. The central limit theorem explains why gamma distributions for high values of ν approximate to Gaussian distributions.

When there is correlation in the surface the distribution will not follow an infinitely divisible family. There is no readily available way of dealing with correlation in non-Gaussian statistics. It is necessary to use a model for the process, to describe the correlation. Oliver [10] has investigated a number of models for correlated gamma processes. This has shown that the effect of area integration is to increase the normalised moments above those of a gamma distribution. The increase, however, only introduces a small deviation from the gamma family. A simple model is introduced in Appendix 7 which, using cumulants, expresses the deviation in terms of an increase in F_3 and F_4. Plots of the third and fourth normalised moments for famliles defined by their values of F_3 and F_4 are shown in Fig. 4. This can be compared to the moment scatter plots of data in Figs. 3*a* and *b*. When it is considered that there are many length scales of correlation over which the area integration is performed, the comparison of the scatter plots of data moments (which are slightly higher than the gamma distribution) with the infinitely divisible familes gives a reasonable match.

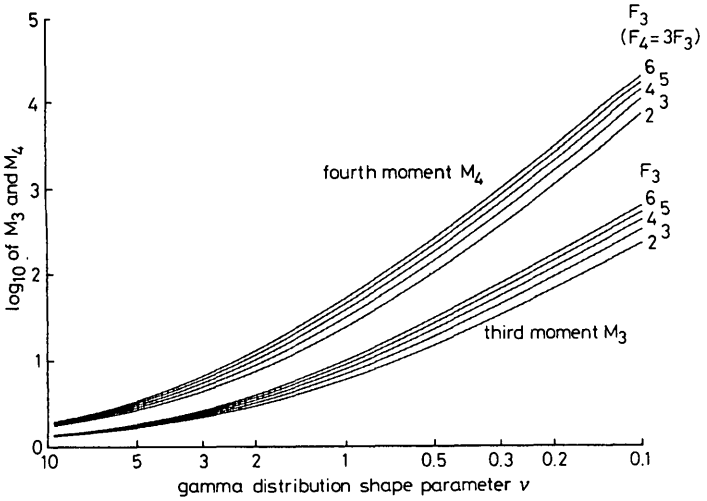

Fig. 4 *Moment plots of the infinitely divisible families with the indicated values of F_3 and F_4, which are defined in the text*
$M_2 = 1 + 1/\nu$

There remains the question of why we expect the very high resolution reflectivity to be gamma distributed. This may be explained in terms of very widely spaced scatterers, where the moments of the reflectivity PDF may be expressed in terms of the scatterer moments as

$$M_n = pMs_n \tag{10}$$

where M_n is the nth reflectivity moment, Ms_n is the nth moment of a typical scatterer and p is the probability of there being a scatterer in an elemental area.

The normalised moments are therefore

$$M_{n(norm)} = Ms_{n(norm)} p^{1-n} \tag{11}$$

The normalised moments of a gamma distribution are

$$M_{n(norm)} = \frac{\Gamma(\nu+n)}{\nu^n \Gamma(\nu)} \simeq (n-1)!\nu^{1-n} \quad \text{for small } \nu \tag{12}$$

Both eqns. 11 and 12 are dominated by the behaviour of p^{1-n} or ν^{1-n} for small values of p or ν, thus suggesting that the gamma distribution is a good model for the very high resolution reflectivity. On the basis of the arguments above it is understandable why the gamma distribution can be used for the modulation component of clutter and also why it slightly underestimates the moments.

2.3 Empirical modelling of ν

For the effective application of the compound K-distribution model it is necessary to understand its sensitivity to radar parameters and environmental conditions. An initial appreciation may be obtained from range–time–intensity plots of the underlying modulation of clutter as shown in Figs. 5*a* to *f*. These indicate how the clutter structure is dependent on radar polarisation, sea state and grazing angle. Fig. 5*a* is taken looking at 30° to the dominant wave direction, with a sea condition of medium roughness (sea state 3, significant wave height 1 m). The grazing angle is 1°. If this is compared with Fig. 5*b*, where the sea condition is rougher (sea state 4, significant wave height 2 m) and the radar is looking upwind, we find that in the latter the wave pattern is more pronounced and the polarisation change has less effect on the clutter. The calm sea plot, Fig. 5*c*, shows both vertical and horizontal polarisation with large spikes of a few seconds duration giving the dominant return. Figs 5*a* to *c* all show a grazing angle in the region of 1°. If this is reduced to 0.1°, as shown in Fig. 5*d* for a rough sea (sea state 5), the well defined wave structure of Fig. 5*b* becomes concentrated into spikes of much higher amplitude (relative to the overall mean). However, there is still a fairly regular structure. Occasionally there is very long-wavelength swell present in the sea wave spectrum. It may not be easily identified visually, but the grazing incidence radar backscatter is dominated by its effects. Fig. 5*e* shows an averaged plot at 1° incidence looking into the swell. The sea roughness is medium (sea state 3) but the swell produces a very clear pattern. As can be seen, the sea wavelength is much longer than any of the other plots. An interesting effect is the dependence of the structure on viewing aspect. Looking down the swell propagation direction produces a plot similar to Fig. 5*e*, but looking across the swell direction breaks up the wave pattern (Fig. 5*f*). This can be explained in terms of the radar footprint. Although the range resolution is 4 m, the

crossrange resolution is determined by the beamwidth of 1.2°. At a range of 16 km, used for Figs. 5*e* and 5*f*, the azimuth patch dimension is 320 m. Thus, when looking into the swell, the radar resolves structure greater than 4.2 m. Across the swell, only structure greater than 320 m is resolved, and then not in range but in time as the swell moves through the beam. The 'across swell' picture is therefore not expected to show the wavelike pattern of the 'into swell' pictures.

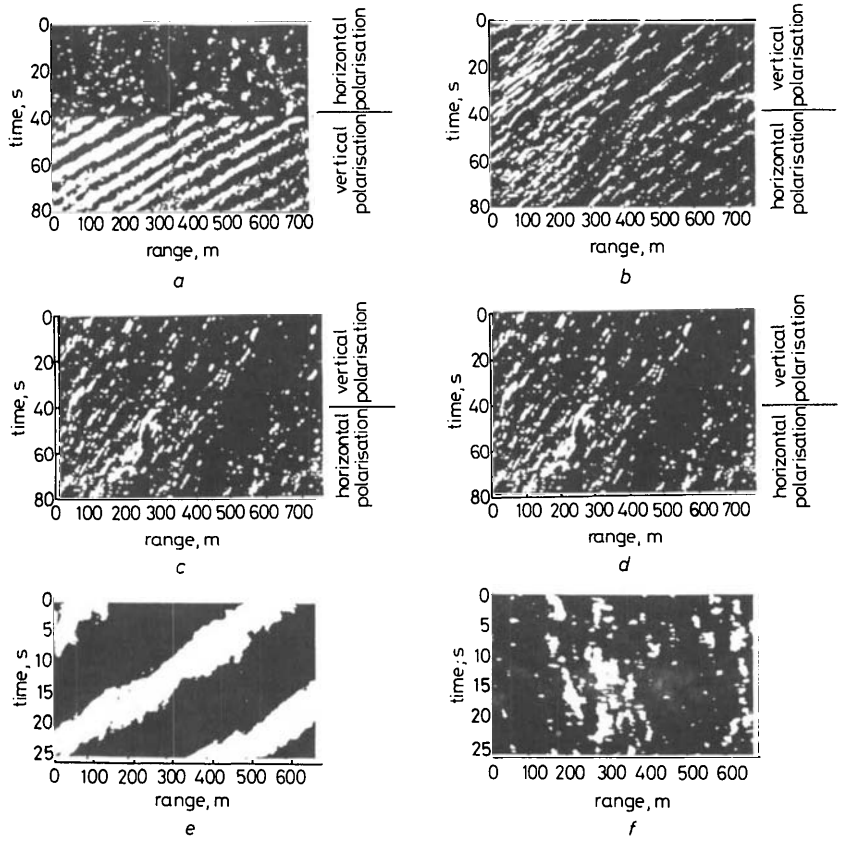

Fig. 5 *Range–time–intensity plots of averaged clutter showing the dependence of the structure on radar and environmental parameters*

a Sea state 3, 30° to upwind, 1° grazing
b Sea state 4, upwind, 1° grazing
c Sea state 1, upwind, 1° grazing
d Sea state 5, upwind, 0.1° grazing
e Sea state 3, upswell, 1° grazing
f Sea state 3, across swell, 1° grazing

The parameterisation of the shape parameter of the K-distribution, v, has been achieved by matching the spread of results to simple functional forms. In this way an empirical model has been derived [1]:

$$\log v = (2/3) \log \varphi + (5/8) \log l + \sigma - k \qquad (13)$$

where v is the estimated value of the shape parameter, l is the across range resolution, φ is the grazing angle in degrees ($0.1° < \varphi < 10°$), σ introduces the aspect dependency as follows:

$\sigma = -\frac{1}{3}$ for up or down swell directions
$\sigma = +\frac{1}{3}$ for across swell directions
$\sigma = 0$ for intermediate directions or when no swell exists

and k describes the polarisation effects with $k = 1$ for vertical and $k = 1.7$ for horizontal polarisation.

It is of interest to note that no significant statistical trend was established for variations with sea state, wind speed or aspect angle relative to wind direction. Also, since each parameter was matched separately to variations with v, complex interdependencies may be missing.

A detailed example of this type of interdependency, which is amenable to analysis, is the effect of range resolution on the statistics. The empirical model described in the previous paragraph is true for a range resolution of 4 m, the value used on all the measurements. However, using the characteristics of the compound K-distribution model, it is possible to synthesise degradations in the resolution [11]. When this is done, different types of clutter, as displayed in Figs. 5*a* to *f*, show different detailed trends of v with resolution. Fig. 6 shows the effect of resolution degradation on a plot of the

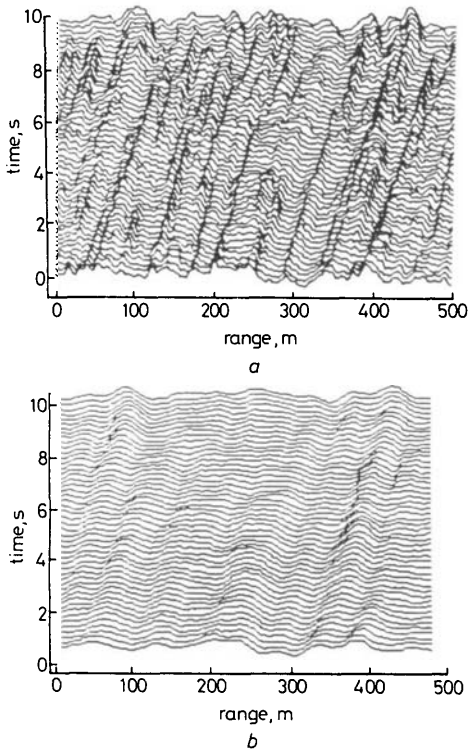

Fig. 6 *Range–time plots of averaged sea clutter showing the effect of different synthesised pulse widths*

a Pulse width = 28 ns
b Pulse width = 200 ns

modulation. It is clear that the short wavelength components are averaged, leaving the longer wavelengths.

2.4 Polarisation characteristics

Before leaving noncoherent clutter it is of interest to examine some polarisation agile recordings, since these provide more insight into the polarisation characteristics evident in Figs. 5*a* to *f*. Polarisation agility is a mode where the transmitted polarisation is switched between vertical (V) and horizontal (H) from pulse to pulse; the receiver measures both polarisations simultaneously in two channels. Fig. 7 shows range–time–intensity plots of

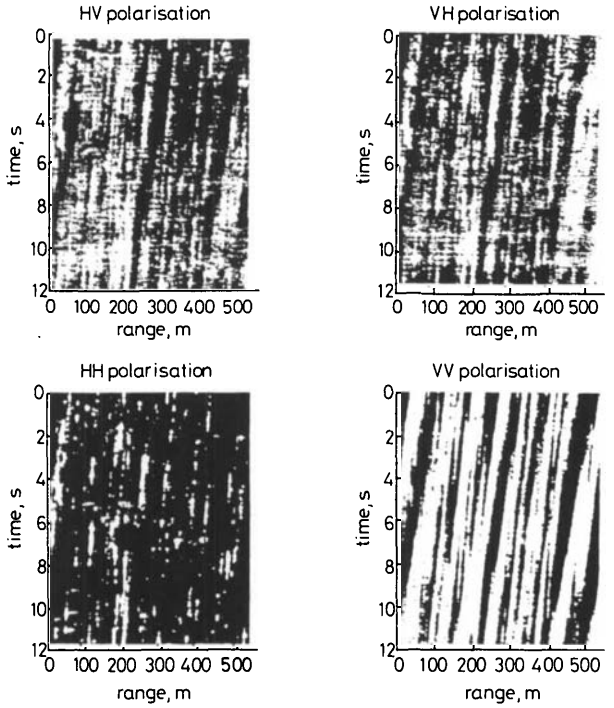

Fig. 7 *Range–time–intensity plots of simultaneous recordings of VV, HH, VH and HV polarisations*
Each pixel is an average over 60 ms

the four polarisation combinations from a 12 s record. The similarity of the VH and HV is evident, as is expected from reciprocity. Also the characteristic spikiness of HH compared to VV can be seen. The dominant spikes on the HH record persist for about one or two seconds. By selecting a range cell containing some of these spikes, the time history of returns from VV and HH can be compared, as shown in Fig. 8*a*. The overall behaviour of the two polarisations is similar, however, the detailed structure is different, indicating that different scatterers are contributing. An example of another area of the record, which does not contain dominant HH spikes is shown in Fig. 8*b*. Here there are occasional large amplitudes in the HH record. These 'bursts' are highly polarisation sensitive and appear to be discrete in nature because of the lack of fluctuation in their time history. The effect of the bursts on the average radar cross-section and the distribution appears to be small compared to the spikes of Fig. 8*a*.

3 Coherent properties of radar sea clutter

In this section we consider the properties of coherent high-range-resolution radar sea clutter with reference to those properties observed noncoherently, as described in the previous section. In particular, we consider the extension of the compound K-distribution description to the case of coherently detected radar sea clutter.

A coherent radar measures the complex received signal rather than just the magnitude. To date, the modelling of coherent non-Gaussian clutter has often consisted of extending the amplitude distribution modelling of noncoherent clutter by measuring the average power spectrum of the coherent signal, followed by matching to a suitable analytic expression. The shortfalls inherent in this approach can be exemplified by considering the simulation of non-Gaussian clutter following this 'Gaussian type of description'. Referring to Fig. 9*a*, wideband Gaussian noise is linearly filtered, followed by a transformation of the amplitude to the required non-Gaussian distribution whilst maintaining the phase. The response of the filter can be adjusted to give the required clutter spectrum after the transformation of amplitude [12]. The simulation has the chosen amplitude distribution (e.g. lognormal, Weibull or K-distribution) and average power spectrum, but it is different from real data in its response to processing. Specifically, time series (or range profiles) of sample spectra do not show the multiplicative nature of the modulation component.

An improved method, which overcomes the main defects of the method of Fig. 9*a* because it is based on the compound approach, is shown in Fig. 9*b*. Here the Gaussian noise is filtered and then modulated by a gamma power distribution to provide a K-distribution for the amplitude. Since this technique (which inciden-

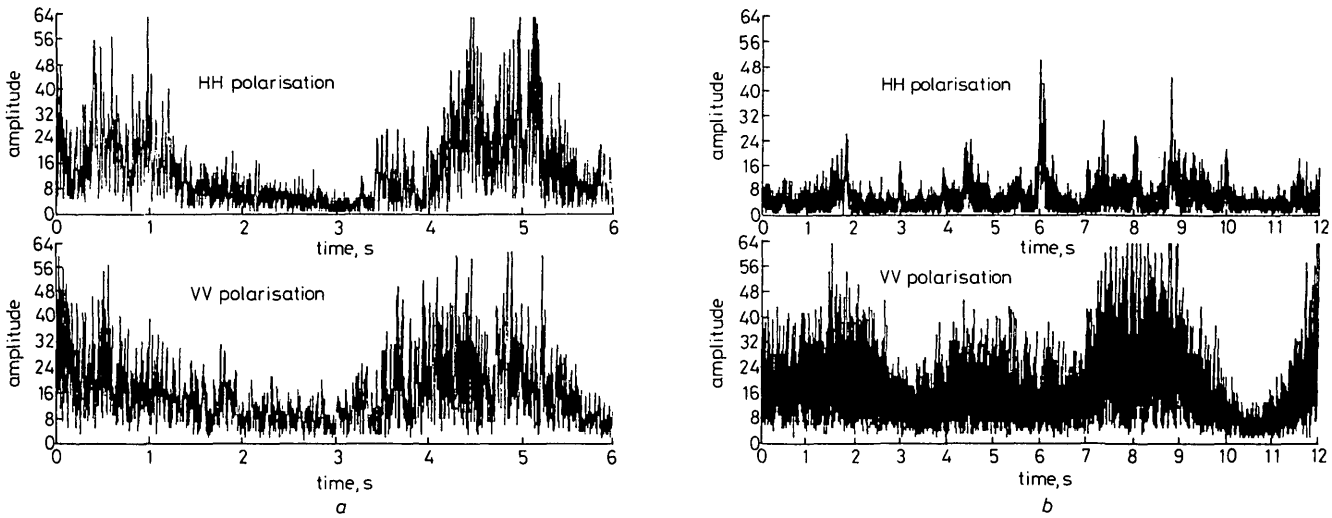

Fig. 8 *Pairs of simultaneous pulse-by-pulse time histories of a clutter range cell at VV and HH polarisations*
(Frequency agility, sea state 3)

tally is not readily applicable to lognormal or Weibull distributions) introduces the non-Gaussian property through the gamma modulation, it produces a much more realistic response to processing. It is not, however, the end of the story, because real data exhibits an interrelationship between the local intensity and the spectral shape.

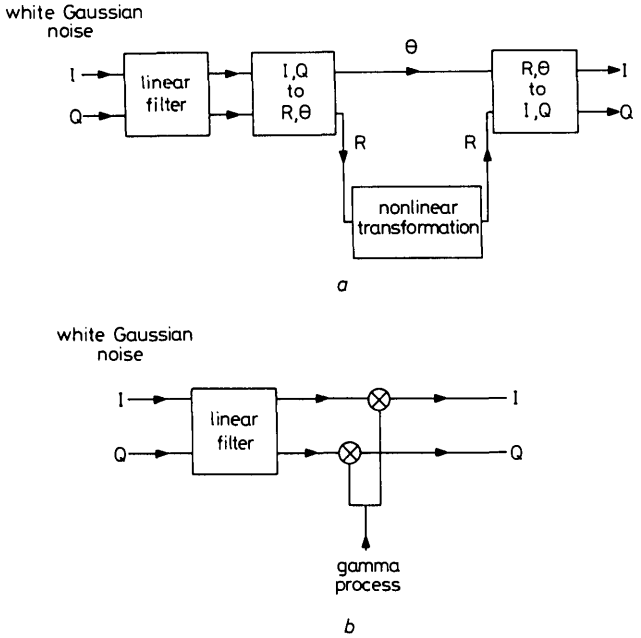

Fig. 9 *Block diagrams of two approaches to the simulation of non-Gaussian clutter*

a Nonlinear transform approach
b Compound approach

This interrelationship is highlighted in Fig. 10, which is a time history of the coherent spectrum from a single range cell. Each spectrum is generated from a 128-point Fourier transform. The polarisation is vertical, the range is approximately 2.5 km and the sea state was observed to be 2. The modulation of intensity is evident as changes in the integrated power of the spectrum as a function of time in Fig. 10. However, the normalised form of the spectrum is not constant, as would be necessary to be consistent with Fig. 9*b*, but has a changing shape and offset. Between approximately 11 and 12 seconds into the time history the spectra exhibit a particularly high Doppler frequency content, which is thought to be a result of local wind gusting effects. This highlights the complexity of the relationship between the intensity modulation and the form of the spectrum, the former being dominated by the swell structure in the sea surface and the latter being additionally affected by the local gusting of the wind. However, despite this complexity it should be noted that the compound modulated Gaussian process is still applicable in the spectral domain and has as direct an effect on the performance of coherent radars as it does on noncoherent radars.

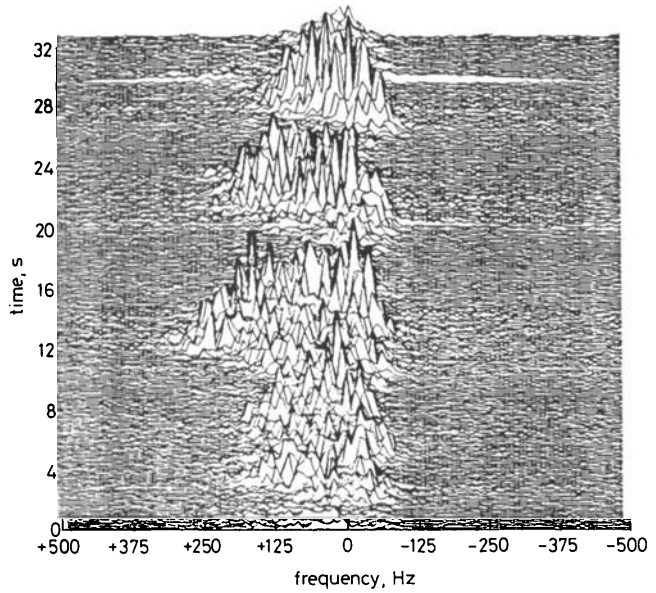

Fig. 10 *Time history of sea clutter Doppler spectra, from a single range cell*

The non-Gaussian nature of the sea clutter spectra is illustrated in Fig. 11. Here the normalised second intensity moments (i.e. the fourth amplitude moments divided by the square of the second amplitude moments) of the Doppler component amplitudes (corresponding to those of Fig. 10) are plotted against frequency and compared to the mean spectrum amplitude. As expected, at the extremes of the frequency span the power is dominated by radar noise because of the relatively small amount of backscatter at these frequencies (or radial velocities). Where there is significant power in the radar return the second moment is larger. This signifies a non-Gaussian distribution and is due to a modulation caused by changes in the average intensity, spectral shape and offset. Further, the value of the second intensity moment changes across the clutter spectrum, indicating that a more sophisticated model than that of filtered Gaussian noise modulated by a gamma distribution is required to describe these observations. Fig. 11 also shows the time averaged spectrum to be somewhat asymmetrical, with a bias towards positive Doppler frequencies. This bias is associated with the direction of the prevailing wind and the largest values of I_2 occur predominantly on the side of the spectrum where the biasing is most pronounced. However, the value of I_2 also takes large values in the opposite wings of the spectrum. This complicates the detection problem still further as the clutter Doppler cells with the least power, where the detection of targets might be expected to occur, have the 'spikiest' signals.

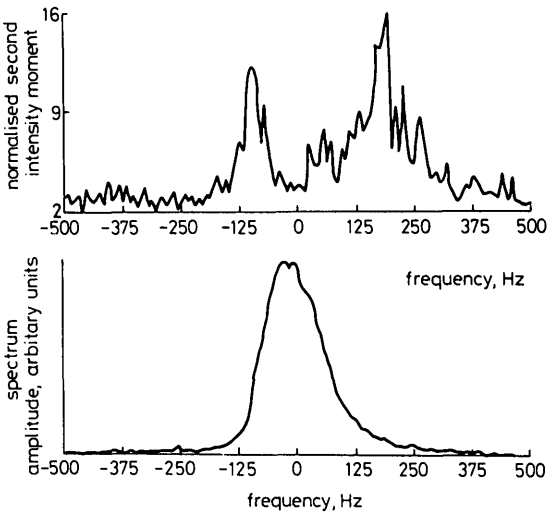

Fig. 11 *Comparison of the sea clutter spectrum, averaged over many time periods, with the normalised second intensity moment for each frequency cell as derived from the sample of time periods, for vertical polarisation*

Fig. 12 shows a plot of the same type as Fig. 11 with the exception that the measurement was made approximately 30 s earlier and that the transmit and receive polarisations were horizontal; otherwise the experimental conditions were identical. Clearly the plots are very

similar in terms of the shape, bandwidth and distribution of the second intensity moment although the values of I_2 are generally higher for horizontal polarisation. In addition, the mean Doppler offset of the averaged spectrum is significantly different for the two polarisations. The dependency of the Doppler offset of the averaged spectrum, for both vertical and horizontal polarisations, on the direction of look of the radar with respect to the sea surface is examined in more detail in Fig. 13.

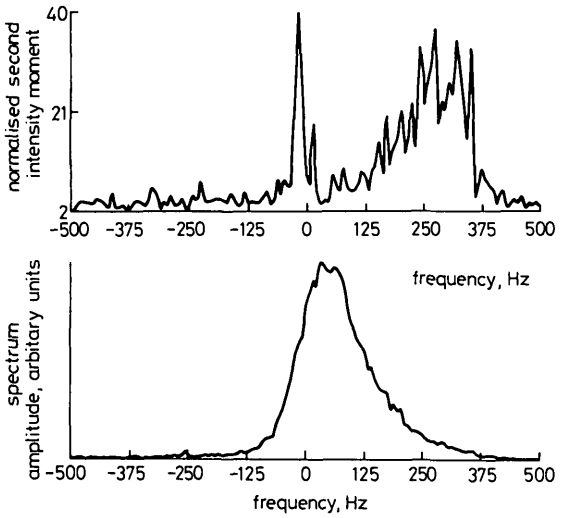

Fig. 12 *Comparison of the sea clutter spectrum, averaged over many time periods, with the normalised second intensity moment for each frequency cell as derived from the sample of time periods, for horizontal polarisation*

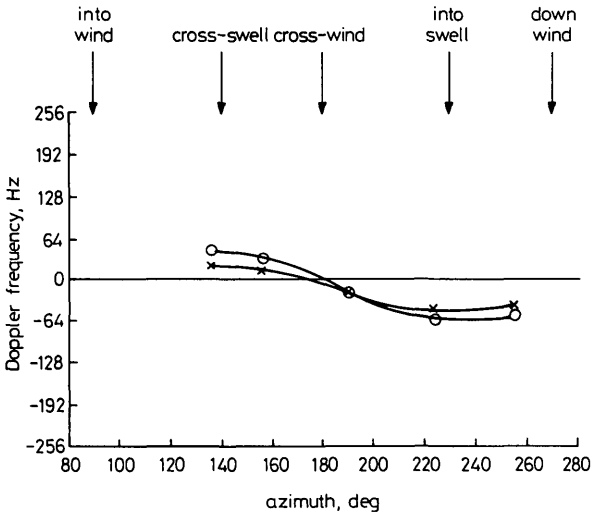

Fig. 13 *Plot showing the trend of mean Doppler frequency against azimuth angle*

○ horizontal polarisation; × vertical polarisation

Here it is shown that data for both polarisations show a cosinusoidal dependence on the direction of the wind, with a zero Doppler offset when looking across-wind. In all cases, except that of crosswind, the Doppler offset is larger for horizontal polarisation than for vertical, suggesting that a different set of scatterers are contributing to the received signals. The characteristics described above are in agreement with observations reported elsewhere [13, 14].

The autocorrelation functions for a number of Doppler frequency components are shown in Fig. 14. Initially, in each case, there is a fast drop-off which is followed by a slower periodic decay. The initial fast decay can be associated with the speckle component of the compound K-distribution model, and the slower periodic decay may be associated with the modulation. Similar effects on performance to those observed with non-coherent detection are therefore expected for high-resolution coherent processing. It is thus clear that the statistical and correlation properties of range Doppler cells must be taken into account in the design and optimisation of coherent radar processors operating in a sea clutter environment.

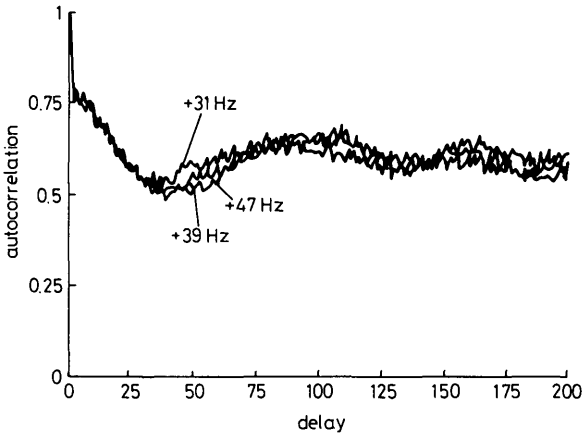

Fig. 14 *Temporal autocorrelation functions of individual range cells plotted against delay measured in units of spectral sampling time (128 ms)*

4 Forward scattering

Any target situated on or close to the sea surface is illuminated by radiation coming directly from the radar and also by radiation reflected from the surface of the sea. Interference at the target, and on the reciprocal path, causes fluctuations in the RCS and distorts the phase front, thus affecting the detection and tracking performance of radars. If the sea were a flat conducting surface, the interference would cause a lobing structure in height; parts of the target at the maxima of the lobing would be enhanced by 12 dB, and parts at the minima would give zero return. In practice, the sea has a dynamic rough surface of complex dielectric. The reflected wavefront is perturbed by the variations in waveheights and therefore fluctuates in both amplitude and phase. The forward reflected wave is generally represented at a point by a coherent and an incoherent component (ρ_c and ρ_i respectively). The ratio of ρ_c to the RMS value of ρ_i depends upon the surface roughness, the EM frequency and the grazing angle. The distribution of ρ_i is often considered to be Rayleigh, which leads to a Ricean distribution at the target (after addition to ρ_i of ρ_c and the direct wave). Therefore, assuming reciprocity, the return signal from a point target viewed monostatically has a Rice-squared distribution. For a distributed target further knowledge of the forward reflected wavefront is required, in particular the spatial coherence. Also, to predict the performance of radars using multiple pulses for detection, a knowledge of the temporal correlation properties is necessary.

4.1 Experimental observations

In this section the scattering characteristics of the wavefront reflected in the forward direction from the surface of the sea are considered via the analysis of experimental data. In particular, we examine the spatial and temporal coherence properties. To investigate these phenomena in a relatively controlled manner a series of experiments have been conducted in 'open sea' conditions, which allows the inclusion of long wavelength sea swell com-

ponents in the scattering surface. Fig. 15 shows the experimental geometry. Measurements were made of radar backscatter from a corner reflector of known free-space echoing area positioned at various heights above the sea surface (1–4 m). The radar was situated at a height of approximately 80 m and the slant range from the radar to the target was approximately 5600 m.

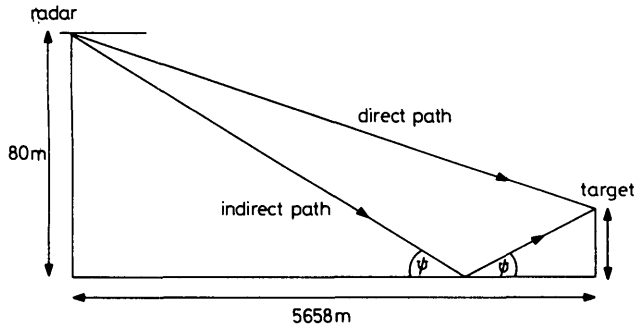

Fig. 15 *Multipath measurement geometry*

Fig. 16 shows the received amplitude time history for a period of approximately 9 minutes, from a measurement made over a relatively calm sea (sea state 1). Each data point has been averaged over 1 s (for a radar PRF of 1 kHz). During this measurement run the corner reflector was slowly raised and lowered at a constant rate giving rise to a lobing structure, which results from the interference of the direct and reflected signals. From the deep nulls in this plot it may be deduced that the coherent reflection coefficient ρ_c is close to unity. The incoherent term ρ_i is small, although not insignificant, and is due to the many small but random phase shifts introduced by the surface roughness.

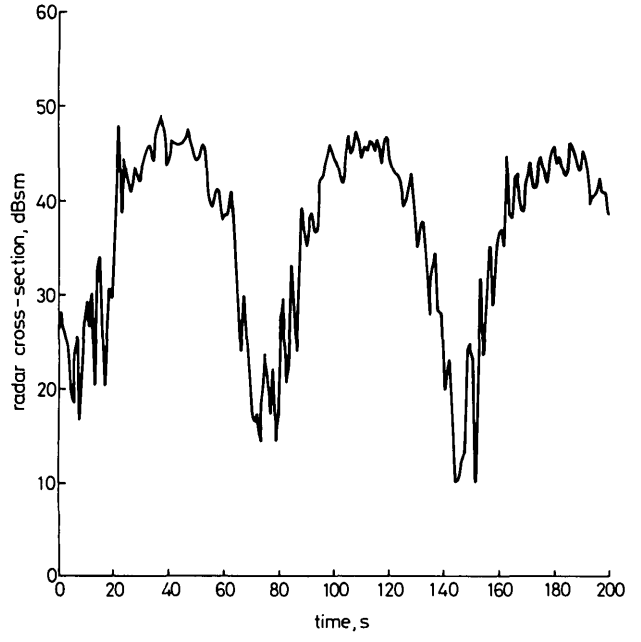

Fig. 16 *Radar cross-section of a reflector (free space RCS = 36 dBsm) as measured undergoing vertical motion over a smooth sea*

In contrast, Fig. 17 shows a similar plot but for a rougher sea (sea state 4). In this figure there is no discernible lobing structure, which, if present, would appear on the same timescale as in Fig. 16. This suggests that the coherent term is close to zero and that the incoherent term is dominating the scattering. Fig. 17 also shows a decorrelation time of about 5 s. This time is related to that which is taken on average for a point on the sea surface to change in height by $\lambda/(2 \sin \psi)$, where ψ is the grazing angle of the illumination. Thus the decorrelation time is dependent on both the RMS waveheight and the dominant wave frequency, and this is different for swell and for wind wave dominated sea spectra.

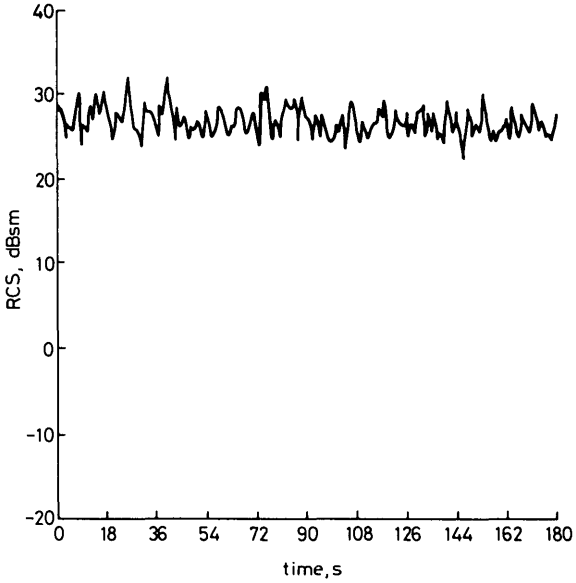

Fig. 17 *Radar cross-section of a corner reflector measured undergoing vertical motion over a rough sea*

If the corner reflector is held at a constant height above the sea surface the resulting time history may be utilised to determine the statistical properties of the received signal. In Fig. 18 the normalised third and fourth amplitude moments, evaluated for a number of different sea states, are plotted against the normalised second moment and are compared with those of a Rice-squared distribution. Clearly, theory and experiment are in excellent agreement and our earlier description of the single point statistics for this scattering is found to be accurate in this configuration.

To examine spatial coherence, two active 'repeater' targets were used, one fitted with a delay line to separate the target responses. Fig. 19 shows a plot of the time history of the backscatter from the two targets when

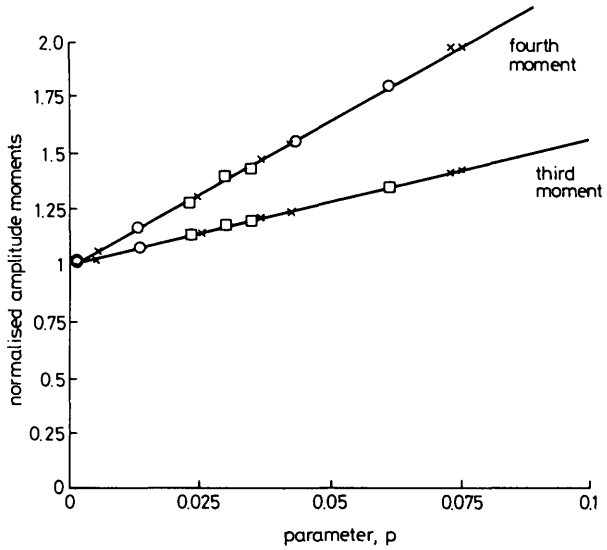

Fig. 18 *Comparisons of normalised third and fourth amplitude moments of the fluctuations of point targets in multipath environments with the moments of Rice-squared distributions*

Lines correspond to Rice-squared distributions, points to data measurements
□ J-band; ○ I-band; × I-band
Normalised second moment = $2 - 1/(1 + p)^2$

separated horizontally by 2.4 m. This shows a high degree of correlation between the two target returns. Fig. 20 is a similar plot with a vertical separation of 1.1 m (this is the spacing between maxima of the lobing structure). The large difference between the traces in Fig. 20 indicates that the forward reflected wavefront decorrelates within 1.1 m in the vertical plane.

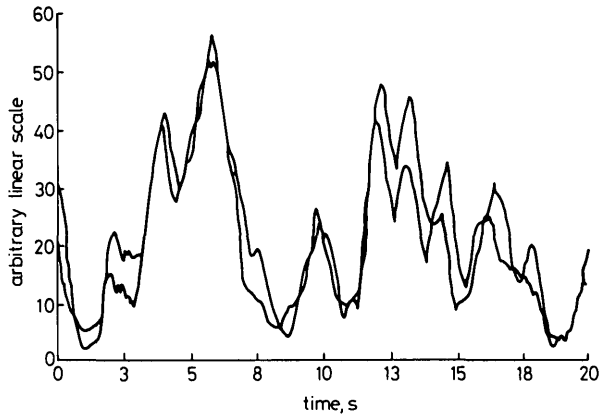

Fig. 19 *Overlayed plots of simultaneous measurements of the fluctuating radar returns from point targets in a multipath environment separated by 1.1 m in a horizontal direction*

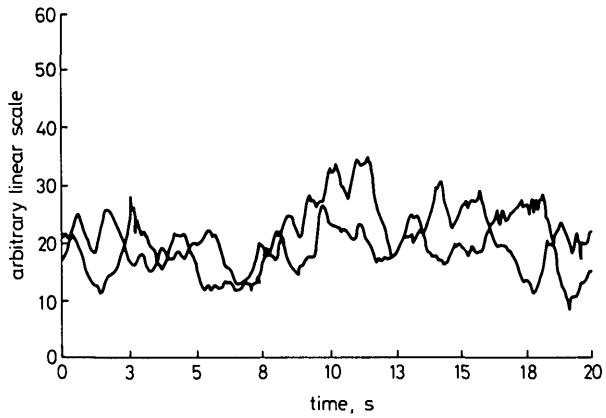

Fig. 20 *Overlayed plots of simultaneous measurements of the fluctuating radar returns from point targets in a multipath environment separated by 1.1 m in a vertical direction*

4.2 Modelling

To apply these results to different geometries or sea conditions it is necessary to develop a physical model. The existing theory for forward scattering is based upon the Kirchoff, or diffraction, integral [15] where the scattered field from any point on the surface is approximated by that which would be scattered if the surface were a plane at a tangent to the point. For plane-wave illumination a change in sea surface height of h introduces a phase change of $4\pi h \sin \psi/\lambda$ in the forward specular scattered field (ψ is the grazing angle, λ is the EM wavelength). For analysis of the coherent term in the scattered field it is assumed that all contributions come from the first Fresnel zone. Thus there is a plane illuminating and scattered wave, and the coherent reflection coefficient is given by

$$\rho_c = \langle e^{i4\pi h \sin \psi/\lambda} \rangle \tag{14}$$

If a Gaussian distribution is used for the sea surface height, the relationship of ρ_c to the RMS waveheight may be calculated [15].

The analysis of the distribution of the scattered field is based upon the assumption of many independent scatterers in the illuminated patch. In the limit of a large number of scatterers, with the constraint of a constant ratio of coherent to incoherent power, the amplitude of the forward-scattered field is Ricean distributed. This is consistent with the Rice-squared distribution for the backscattered field from a point target in multipath, as shown in Fig. 18. In cases where the contributing area of the surface resolves the gross sea wave structure, an approach similar to that used earlier for the bunching of scatterers leads to the generalised K-distribution for the forward-scattered field [16].

Evaluation of the mean square magnitude or spatial correlation of the incoherent field requires knowledge of the area of sea contributing. Arguments based on the first Fresnel zone are not applicable, and an approach using a geometric optics approximation is usually applied. An area is defined, called the 'glistening surface' [e.g. 17]; this area includes all points where specular reflection of a ray from the transmitter to the target via the sea surface is possible with a wave slope of less than g. (A suitable value of g may be derived from the sea surface spectrum.) The scattered incoherent field is assumed to come from within this area, and is modelled by the sum of contributions from many independent scatterers. It may then be written as

$$\rho_i \propto \sum_{n=1}^{N} \frac{a_n}{\alpha_n \beta_n} e^{i\varphi_n} \tag{15}$$

where a_n and φ_n are the amplitude and phase of the nth scatterer. α_n is its range from the transmitter, β_n is its range from the target. The summation covers all scatterers within the glistening surface.

We may extend this approach to the spatial autocorrelation function of ρ_i by using the independence of a_n and φ_n, and the uniform distribution of φ between 0 and 2π. Thus the spatial autocorrelation function of ρ_i is

$$R(\delta r) = \langle \rho_i(r)\rho_i^*(r + \delta r) \rangle \propto \frac{N\langle a_n^2 \rangle}{S_{gs}} \int ds \frac{e^{i\varphi(\delta r)}}{\alpha^2 \beta(r)\beta(r + \delta r)} \tag{16}$$

where

$$\varphi(\delta r) = \frac{2\pi}{\lambda} [\beta(r + \delta r) - \beta(r)] \tag{17}$$

with the integral taken over the glistening surface, which has area S_{gs}.

This function has been evaluated numerically using the parameters from the experimental geometry described above, and a maximum wave slope of $g = 0.1$. The result is plotted in Fig. 21. It is clear that the model predicts the decorrelation distance for vertical separation to be much less than that for horizontal separation. This is consistent with experiment (Figs. 19 and 20). Qualitatively the effect is due to the projection of the glistening surface on to the plane of propagation being much larger in the vertical than the horizontal dimension. (This is as observed, for example, when viewing the moon reflected in a shimmering lake.) This translates to a diffraction pattern which decorrelates in a shorter distance in the vertical than horizontal direction.

Implicit in the derivation above is the assumption that the distribution of slopes is uniform up to a cutoff of g. A more reasonable description is a Gaussian distribution of slopes. To modify the analysis to account for this, the

glistening surface boundary would be replaced by a weighting of the amplitudes of the a_n, the weighting derived from the probability density associated with the required slope at each point.

When the wave slope distribution is not isotropic, for example when there is a dominant swell, the shape of the glistening surface is modified. This changes the scattered spatial correlation function from the form shown in Fig. 21. Another important consideration for extending the

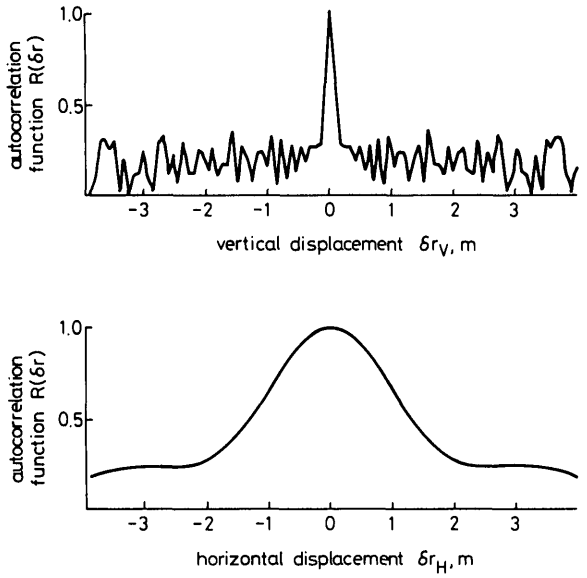

Fig. 21 *Spatial autocorrelation function of the forward-scatter incoherent reflection coefficient, showing the shorter correlation distance in the vertical compared to horizontal direction based on the theory outlined in Section 4.2*

analysis is for the case where the glistening surface is smaller than the swell wavelength in both dimensions. Here the assumption of independent scatterers breaks down. The effect is to introduce a residual spatial correlation in the incoherent scattered field caused by the component of slope that is constant across the glistening surface.

This concludes the discussion on a physical model to describe the results presented in Section 4.1. All the properties of the forward-scattered field as described are important when considering the radar backscatter from complex targets. Analysis of the effects, particularly of the correlation properties, is only at an early stage.

5 Conclusions

In this paper we have shown how many of the characteristics of microwave radar scattering from the ocean surface can be statistically modelled in a phenomenological way, where the observed fluctuation properties are described without resort to electromagnetic scattering theory. The compound form of the K-distribution has been used to describe high-resolution noncoherent radar sea clutter. It has been shown how the same type of approach may be applied, albeit in a more qualitative way, to coherent clutter and forward scattering. The claim that this form of modelling encapsulates the properties of radar scattering that are important to radar design and performance analysis is justified in the companion second part to this paper.

6 References

1 WARD, K.D.: 'A radar sea clutter model and its application to performance assessment', *IEE Conf. Publ. 216*, Radar-82, 1982, pp. 204–207
2 BAKER, C.J., WARD, K.D., and WATTS, S.: 'The significance and scope of the compound K-distribution model for sea clutter', *IEE Conf. Publ. 281*, Radar-87, 1987, pp. 207–211
3 WATTS, S., BAKER, C.J., and WARD, K.D.: 'Maritime surveillance radar. Part 2: Detection performance prediction in sea clutter', *IEE Proc. F, Radar & Signal Process.*, 1990, **137**, (2), pp. 63–72
4 BAKER, C.J., and WARD, K.D.: 'I-band multipath propagation over the sea surface'. AGARD Conf. No. 419, 1987, pp. 25-1 to 25-4
5 BAKER, C.J., PINK, J.M., and TOUGH, R.J.A.: 'A statistical model for radar target detection in clutter'. Proc. IEEE National Radar Conf., 1988, pp. 241–245
6 JAKEMAN, E., and TOUGH, R.J.A.: 'Non-Gaussian models for the statistics of scattered waves', *Adv. Phys.*, 1988, **37**, pp. 471–529
7 OLIVER, C.J.: 'The representation of correlated clutter textures in coherent images', *Inverse Probl.*, 1988, **4**, pp. 843–866
8 LEWINSKI, D.J.: 'Nonstationary probabilistic target and clutter scattering models', *IEEE Trans.*, 1983, **AP-31**, (3), pp. 490–498
9 JAKEMAN, E.: 'On the statistics of K-distributed noise', *J. Phys. A*, 1980, **13**, pp. 31–48
10 OLIVER, C.J.: 'Correlated K-distributed clutter models', *Opt Acta*, 1985, **32**, pp. 1515–1547
11 WATTS, S., and WARD, K.D.: 'Spatial correlation in K-distributed sea clutter', *IEE Proc. F, Commun., Radar & Signal Process.*, 1987, **134**, (6), pp. 526–532
12 CONTE, E., GALATI, G., and LONGO, M.: 'Exogenous modelling of non-Gaussian clutter', *JIERE*, 1987, **57**, pp. 151–157
13 PIDGEON, V.W.: 'Doppler dependence of radar sea return', *J. Geophys. Res.*, 1968, **73**, pp. 1333–1341
14 MELNICHUK, Yu.V., and CHERNIKOV, A.A.: 'Spectra of radar signals from the sea surface for different polarisations', *Izvestia Atmos. and Ocean Phys.*, 1971, **7**, pp. 17–24
15 BECKMAN, P., and SPIZZICHINO, A.: 'The scattering of electromagnetic waves from rough surfaces' (Pergamon Press, 1963)
16 JAKEMAN, E., and TOUGH, R.J.A.: 'Statistical models of low-angle forward-scattering of microwaves', *IEE Conf. Publ. 281*, Radar-87, 1987, pp. 568–573
17 BARTON, D.: 'Low angle radar tracking', *Proc. IEEE*, 1974, **62**, pp. 687–704

7 Appendix: Correlated gamma model

In Gaussian noise, correlation may be introduced by linear filtering. This may be considered as the weighted average of independent Gaussian samples, i.e.

$$x_i = \frac{1}{N} \sum_{j=0}^{N-1} w_j y_{i-j} \tag{18}$$

where y_i are the independent samples (white noise), x_i are the correlated samples (coloured noise), and w_i are the filter weights. In Gaussian noise this is possible because the weighted average of Gaussian variates is always Gaussian. For a gamma distribution of y_i, the x_i are only gamma if all w_j are the same. This limits the type of correlation introduced, but can be used to illustrate the increase in F_i (eqn. 7) when correlated samples are summed. For a filter of length N

$$v_x = N v_y \tag{19}$$

where v is the gamma distribution shape parameter.

Having generated the correlated gamma samples x_i, these may be averaged to investigate the effect on the moments.

Summing the consecutive values of x

$$x_s = x_i + x_{i+1} = \left(y_{i-N-1} + 2 \sum_{j=0}^{N-2} y_{i-j} + y_{i+1} \right) \Big/ N \tag{20}$$

The normalised cumulants of x_s are

$$K_i = \frac{2^{1-i} + (N-1)}{N^i v^{i-1}} (i-1)! \tag{21}$$

The values of F_i (as defined in main text) after this summing of the correlated variates are

$$F_i = \frac{N^{i-2}(2^{1-i} + (N-1))}{(N-0.5)^{i-1}}(i-1)! \tag{22}$$

(For $N = 2$, this gives $F_3 = 2.2$, $F_4 = 8$.)

For a gamma distribution, the relationship is

$$F_{i(\text{gamma})} = (i-1)! \tag{23}$$

Therefore, the effect of summing correlated variates with this model is to increase the values of F_i. This modifies the moments as shown in Fig. 4.